AIMS Energy, 13(5): 1301–1319.
DOI: 10.3934/energy.2025048
Received: 30 June 2025
Revised: 23 September 2025
Accepted: 09 October 2025
Published: 16 October 2025

https://www.aimspress.com/journal/energy

*Research article*

# Research on frequency regulation of wind turbines assisted by flywheel energy storage virtual synchronous machine

**Lu Wang[1], Tianshu Qiao[2], Chen Chen[3], Yu Zhao[1] and Yibing Liu[2,*]**

[1] Shenzhen Energy Nanjing Energy Holding Co., Ltd., No. 99, Baima Avenue, Baima Town, Lishui District, Nanjing, Jiangsu, China
[2] School of Energy and Power Engineering, North China Electric Power University, Beinong Road No.2, Beijing, China
[3] China Datang Corporation Technical and Economic Research Institute, No. 8 Chengzhen Kuangou, Beijing, China

* **Correspondence:** Email: lyb@ncepu.edu.cn; Tel: +13911293869.

**Abstract:** By using power-type flywheel energy storage to assist the operation of newly built wind turbines, their frequency regulation capability can be improved. This paper proposed a virtual synchronous generator (VSG) model with flywheel energy storage and a wind turbine model and simulated the frequency characteristics of the regional power grid of these models. The results showed that the addition of the flywheel energy storage system improves the frequency regulation capability of the newly built wind turbines, enabling wind turbines to perform frequency regulation and alleviating the problem of grid frequency deterioration caused by large-scale access to wind power. Based on the simulation experiments conducted using the measured data from wind farms, compared with the traditional operating condition, the integration of a flywheelVSG system with a capacity equivalent to 10% of the wind power capacity can reduce the power grid frequency deviation by approximately 11%.

**Keywords:** flywheel energy storage; wind turbine; frequency characteristics; simulation analysis; modeling

**Nomenclature:** $J$: generator rotor moment of inertia, N·m; $\omega_m$: generator rotor mechanical angular velocity, rad/s; $T_m$: prime mover mechanical torque, N·m; $T_e$: generator electromagnetic torque, N·m; $K_D$: generator damping coefficient; $\Omega_m$*: generator rotor angular frequency per unit value; $\Omega_N$: rated mechanical angular frequency; $\delta_m$: generator power angle; $J_{VSG}$: VSG rotor moment of inertia; $K_{VSG}$: VSG damping coefficient; $\omega$*: rotor mechanical angular frequency per unit value; $\omega_0$: rotor rated mechanical angular frequency; $\delta_{VSG}$: VSG power angle; $S_{VSG}$: VSG rated capacity, W; $W_N$: virtual rotor kinetic energy at rated speed of VSG; $T_{VN}$: rated torque at rated speed of VSG; $P_{Vm}$*: mechanical power per unit value; $\Delta P_{Vm}$*: mechanical power increment per unit value; $P_{Ve}$*: electrical power per unit value; $\Delta P_{Ve}$*: electrical power increment per unit value when power angle changes; $\Delta\omega$: angular frequency increment per unit value; $D_{VSG}$: VSG damping coefficient; $\Delta\delta_{VSG}$: power angle increment; $E$: VSG terminal voltage, V; $U_g$: grid voltage, V; $Z$: output impedance; $\Lambda$: impedance angle; $\Delta\Lambda$: impedance angle increment; $S_E$: VSG synchronizing power coefficient; $\omega_n$: natural oscillation frequency; $\xi$: damping ratio; $\rho$: air density, kg/m³; $C_p$: power coefficient; $S$: wind turbine blade swept area, m²; $\beta$: pitch angle; $v_w$: current wind speed, m/s; $H_g$: wind wheel inertia time constant; $H_t$: generator inertia time constant; $\omega_r$: rigid shaft rotation angular velocity; $T_m$: wind turbine mechanical torque; $T_e$: generator electromagnetic torque; $D_r$: rigid shaft damping coefficient; $u_d$: D-axis component of motor voltage V, V; $u_q$: Q-axis component of motor voltage V, V; $i_q$: motor stator current, A; $L$: shaft synchronous inductance, H; $R_s$: stator winding resistance, Ω; $\psi_f$: rotor flux, Wb; $\omega_e$: rotor angular velocity, rad/s; $\omega_m$: rotor mechanical angular velocity, rad/s; $p$: number of permanent magnet synchronous motor rotor pole pairs; $B$: motor viscous friction coefficient, rad; $J$: motor rotor moment of inertia, kg·m²; $R_1$: primary frequency regulation coefficient of thermal power unit; $G_1(s)$: comprehensive transfer function of thermal power unit; $G_2(s)$: flywheel energy storage system transfer function; $G_3(s)$: comprehensive transfer function of wind turbine; $K_1$: power generation ratio of thermal power unit; $K_2$: power generation ratio of wind turbine; $K_3$: flywheel energy storage VSG capacity ratio; $M$: equivalent generator rotor time constant; $D$: load damping coefficient; $T_G$: equivalent inertia time constant of the steam turbine, s; $a$: characteristic coefficient of the steam turbine

## 1. Introduction

With the continuous increase in wind power penetration, grid frequency security has become a challenging problem for many countries [1,2]. In response, researchers in the power industry have proposed a variety of different solutions. Among them, the virtual synchronous generator (VSG) technology designs the control logic of power electronic equipment to present output characteristics similar to those of synchronous generators, which can give the generator set or energy storage equipment inertia and enhance its frequency regulation ability when facing active disturbances [3,4]. At present, the main research directions of VSG include the VSG control strategy itself and its application in renewable energy generation and energy storage. For example, reference [5] proposed a VSG control method suitable for the combined operation of photovoltaic (PV) and energy storage systems. This method can improve the overall response speed and accuracy of the unit; compared with conventional VSG control, the response speed of the energy storage equipment with this control method increased by more than 11%. In reference [6], authors proposed an improved VSG control

method, which can enhance the stability of the system during operating condition transitions. For equipment adopting this control method, its critical clearing time (CCT) can be more than doubled compared with that of the traditional control method, demonstrating a remarkably significant effect. In reference [7], authors discussed the selection principles and control performance of virtual parameters in the VSG. This paper obtained the feasible region of VSG control parameters for transient synchronization stability using the Lyapunov direct method, enabling parameter selection to meet the requirements for transient stability based on grid codes and the rate of change of frequency (RoCoF) under large disturbances. In general, power electronic equipment operating in VSG mode has better performance, and research in this field is increasingly receiving attention from the industry.

Flywheel energy storage technology is a long-standing technology that has recently begun to be applied in the power industry. This technology has the characteristics of fast response speed, high control accuracy, large instantaneous power, and excellent frequency regulation performance [8]. The flywheel energy storage system (FESS) can act on the power generation side to improve the frequency regulation capability of the unit or stabilize the frequency fluctuation of the wind farm. It can also operate independently or form a hybrid energy storage power station to directly connect to the grid to provide auxiliary services. It has shown good results in the above application scenarios [9,10]. Based on the operating principle of flywheel energy storage and the control logic of VSG technology, this paper conducts mathematical modeling and analysis of the parameter selection range for the flywheel energy storage-based VSG. Furthermore, using the actual operating data of wind turbines, it adopts simulation research to explore the improvement effect of the flywheel energy storage-based VSG on the frequency regulation capability of wind turbines. The results show that the flywheel energy storage-based VSG can effectively reduce the frequency fluctuation of the power grid containing wind turbines, thereby improving the primary frequency regulation capability of the wind turbines.

## 2. Flywheel energy storage virtual synchronous machine technology

### *2.1. Introduction to flywheel energy storage technology*

Flywheel energy storage is a mechanical energy storage technology that achieves energy storage by converting mechanical energy (expressed as the kinetic energy of the flywheel rotor) and electrical energy. In the early days, this technology was mainly used in kinetic energy recovery, uninterruptible power supply (UPS), and aerospace technology, among others; its application in the power field was relatively late, and related engineering practices have only gradually emerged in the past two decades. For example, in 2011, Beacon Energy Company of the United States put into operation a 40 MW flywheel energy storage frequency regulation power station in Stephentown, New York; in September 2024, Shanxi, China, built a flywheel energy storage independent frequency regulation power station with a total capacity of 30 MW and successfully connected to the grid. In addition, there are currently many similar projects under construction. These power stations are used for frequency modulation (FM). Figures 1a and 1b are real photos of two frequency regulation power stations.

(a) Stephentown FM station

(b) Shanxi Changzhi FM power station

**Figure 1.** Flywheel energy storage power station examples.

The flywheel energy storage frequency modulation power station is composed of multiple groups of flywheel energy storage units. The schematic diagram of a single flywheel energy storage unit is shown in Figure 2, in which the flywheel energy storage unit is installed in an underground cement base. This arrangement can reduce the operating noise and control the degree of harm to the maximum extent when safety accidents such as rotor rupture occur, avoiding damage to personnel and other equipment and property.

The flywheel energy storage unit is usually composed of an outer shell, a rotor, a bearing, a bidirectional motor, a protective cover, a control system, a cooling system, and a power conversion device (PCS). The outer shell is made of high-strength metal material, which wraps other components to form an overall protection; the rotor is the core energy storage component and is placed in a reasonable position after being isolated by the bearing; the bidirectional motor is arranged under the rotor and is protected by a protective cover on the outside; the control system regulates the normal charging and discharging of the flywheel unit; the cooling system ensures that the temperature of each component does not exceed the limit. The entire unit is connected to the power grid through the PCS system to achieve the absorption or release of electric energy.

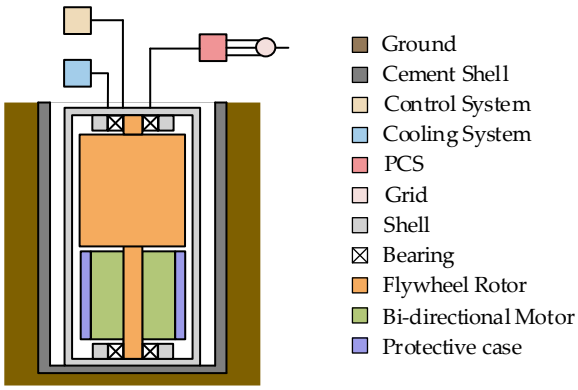


**Figure 2.** Schematic diagram of a flywheel energy storage unit.

### *2.2. Mathematical modeling of a virtual synchronous machine*

The flywheel energy storage VSG simulates the external output characteristics of the synchronous generator, so that the flywheel energy storage system has inertia support capability, thereby improving the overall frequency response performance of the hybrid unit after coupling with wind turbine. Based

on this principle, Figure 3 shows a typical flywheel energy storage VSG control architecture.

The VSG control system acts on the grid-side converter and adjusts the active power and reactive power output according to the input signal. Pref is the active power reference value; $Q_{\text{ref}}$ is the reactive power reference value; $P_{\text{VSG}}$ represents the active power output value of the flywheel energy storage VSG [11]. The motor used in this paper is a permanent magnet synchronous motor (PMSM).

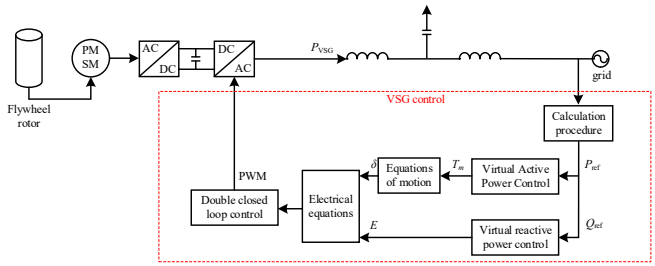


**Figure 3.** Flywheel energy storage VSG control principle diagram.

In a synchronous generator set, the acceleration or deceleration behavior of the generator and the prime mover is due to the imbalance between the electromagnetic torque and the mechanical torque. This dynamic characteristic can be expressed by the motion equation shown in Eq (1):

$$\begin{cases} J\dfrac{d\omega_m}{dt} = T_m - T_e - K_D(\Omega_m^* - 1)\Omega_N \\ \dfrac{d\delta_m}{dt} = (\Omega_m^* - 1)\Omega_N \end{cases} \tag{1}$$

When the flywheel energy storage VSG pole pair number is set to 1, its induced electromotive force angular frequency is equal to the rotor mechanical angular frequency, and Eq (1) can be rewritten as Eq (2):

$$\begin{cases} J_{\text{VSG}}\dfrac{d\omega_m}{dt} = T_m - T_e - K_{\text{VSG}}(\omega^* - 1)\omega_0 \\ \dfrac{d\delta_{\text{VSG}}}{dt} = (\omega^* - 1)\omega_0 \end{cases} \tag{2}$$

According to the generator convention, the inertia time constant $H$ is used to characterize the rotor kinetic energy stored in the rotating body. The inertia coefficient $H_{\text{VSG}}$ of the flywheel energy storage VSG can be expressed by Eq (3):

$$H_{\text{VSG}} = \frac{1}{2}\frac{J\omega_0^2}{S_{\text{VSG}}} \tag{3}$$

The time required for a synchronous generator to start from a stationary state is $2H_{\text{VSG}}$, and the energy balance equation of its starting process is shown in Eq (4):

$$\begin{cases} W_N = \dfrac{1}{2}J_{\text{VSG}}\omega_0^2 \\ W_N = \int_0^{2H_{\text{VSG}}} T_{\text{VN}}\omega(t)dt \end{cases} \tag{4}$$

The normalized rotor motion equation of flywheel energy storage VSG can be derived from Eqs (2–4), and its incremental form can be obtained after rewriting as shown in Eq (5):

$$\begin{cases} P_{\mathrm{Vm}}^{*}+\Delta P_{\mathrm{Vm}}^{*}-\left(P_{\mathrm{Ve}}^{*}+\Delta P_{\mathrm{Ve}}^{*}\right)=2H_{\mathrm{VSG}}\dfrac{d\left(\omega^{*}+\Delta\omega^{*}\right)}{dt}+D_{\mathrm{VSG}}\left(\omega^{*}+\Delta\omega^{*}-1\right) \\ \dfrac{d\left(\delta_{\mathrm{VSG}}+\Delta\delta_{\mathrm{VSG}}\right)}{dt}=\left(\omega^{*}+\Delta\omega^{*}-1\right)\omega_{0} \end{cases} \tag{5}$$

When connected to the grid, this relationship can be expressed by Eq (6):

$$\Delta P_{\mathrm{Ve}}^{*}=\frac{EU_{g}}{S_{\mathrm{VSG}}Z}\cos(\Lambda)\Delta\Lambda=S_{E}\Delta\Lambda \tag{6}$$

According to Eqs (5) and (6), the relationship between VSG active power and frequency can be derived as shown in Eq (7):

$$\frac{\Delta\omega^{*}(s)}{\Delta P_{\mathrm{Vm}}^{*}(s)}=\frac{s}{2H_{\mathrm{VSG}}s^{2}+D_{\mathrm{VSG}}s+S_{E}\omega_{0}} \tag{7}$$

By rewriting Eq (7), the relationship between input power and output power in VSG can be obtained, as shown in Eq (8):

$$\frac{\Delta P_{\mathrm{Ve}}^{*}(s)}{\Delta P_{\mathrm{Vm}}^{*}(s)}=\frac{S_{E}\omega_{0}}{2H_{\mathrm{VSG}}s^{2}+D_{\mathrm{VSG}}s+S_{E}\omega_{0}} \tag{8}$$

We can further get:

$$\frac{\Delta P_{\mathrm{Ve}}^{*}(s)}{\Delta P_{\mathrm{Vm}}^{*}(s)}=\frac{\omega_{n}^{2}}{s^{2}+2\xi\omega_{n}s+\omega_{n}^{2}} \tag{9}$$

Among them, the meanings of $\omega_{\mathrm{n}}$ and $\xi$ are as shown in Eq (10):

$$\begin{cases} \omega_{n}=\sqrt{\dfrac{\omega_{0}S_{E}}{2H_{\mathrm{VSG}}}} \\ \xi=\dfrac{D_{\mathrm{VSG}}}{4}\sqrt{\dfrac{2}{\omega_{0}S_{E}H_{\mathrm{VSG}}}} \end{cases} \tag{10}$$

From Eqs (8) and (10), it can be seen that the damping ratio $\xi$ is a key parameter in the design of the VSG system, and its value is affected by $H_{\mathrm{VSG}}$ and $D_{\mathrm{VSG}}$. Figure 4 shows the root locus diagram when $H_{\mathrm{VSG}}$ and $D_{\mathrm{VSG}}$ change.

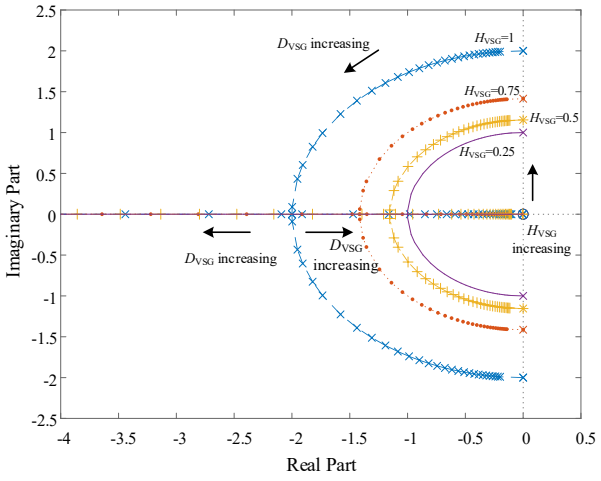


**Figure 4.** Root locus plot.

As shown in Figure 4, when $D_{VSG}$ is a constant, as $H_{VSG}$ increases, the characteristic root moves away from the imaginary axis, and the shorter the system adjustment time, the better the stability; when $H_{VSG}$ is a constant, as $D_{VSG}$ increases, its characteristic root gradually becomes a real pole, and the dynamic response of the system slows down. By adjusting the size of the virtual parameters, the dynamic response of VSG can present underdamped, critically damped, or overdamped characteristics. The underdamped system has a short adjustment time but overshoot, and the overdamped system has no overshoot but a long adjustment time.

### *2.3. Dynamic response characteristics analysis of a virtual synchronous machine with flywheel energy storage*

When the power change instruction of flywheel energy storage VSG participating in active power regulation is $\Delta P_{Vm}^{*}$, the dynamic response characteristics of flywheel energy storage VSG under different damping ratios are analyzed [12].

1) Overdamping ($\xi > 1$)

When the damping ratio $\xi > 1$, the step response of the flywheel energy storage VSG has no overshoot, and Eq (8) has two real characteristic roots:

$$\begin{cases} p_1 = -\frac{1}{T_1} = -\left(\xi - \sqrt{\xi^2 - 1}\right)\omega_n \\ p_2 = -\frac{1}{T_2} = \left(\xi + \sqrt{\xi^2 - 1}\right)\omega_n \end{cases} \tag{11}$$

Usually, when the damping ratio $\xi >> 1$, the system reaches 98% of the stable value after $aT_1$ ($a \geq 4$) time. Therefore, when overdamped, the response time of the flywheel energy storage VSG is:

$$t_s \approx aT_1 = \frac{a\left(\xi + \sqrt{\xi^2 - 1}\right)}{\omega_n} \approx \frac{2a\xi}{\omega_n} (a \geq 4) \tag{12}$$

At this time, the output power response of the flywheel energy storage VSG is:

$$\Delta P_{Ve}^{*}(t) = \Delta P_{Vm}^{*}\left[1 - \frac{\omega_n}{2\sqrt{\xi^2 - 1}}\left(\frac{e^{-p_1 t}}{p_1} - \frac{e^{-p_2 t}}{p_2}\right)\right] \tag{13}$$

The time domain energy variation of the flywheel energy storage required during the VSG rotor movement is expressed as:

$$E(t) = \int_0^{\infty} [\Delta P_{Vm}^{*} - \Delta P_{Ve}^{*}(t)]\, dt = \frac{\omega_n \Delta P_{Vm}^{*}}{2\sqrt{\xi^2 - 1}}\left[\left(-\frac{e^{-p_1 t}}{p_1^2} + \frac{e^{-p_2 t}}{p_2^2}\right) + \left(\frac{1}{p_1^2} - \frac{1}{p_2^2}\right)\right] \tag{14}$$

When $t \rightarrow \infty$, the maximum flywheel energy storage required for the VSG rotor motion process is:

$$E = \frac{\omega_n \Delta P_{Vm}^{*}}{2\sqrt{\xi^2 - 1}}\left(\frac{1}{p_1^2} - \frac{1}{p_2^2}\right) = \frac{2\xi}{\omega_n}\Delta P_{Vm}^{*} \tag{15}$$

Calculate the second-order derivative of Eq (12) and set the derivative to 0. The maximum value of the energy storage power ($P_{max}$) required by the flywheel energy storage VSG is:

$$P_{\max} = \frac{\omega_n \Delta P_{Vm}^{*}}{2\sqrt{\xi^2 - 1}}\left(\frac{p_2 - p_1}{2p_1 p_2}\right) = \Delta P_{Vm}^{*} \tag{16}$$

2) Critical damping ($\xi = 1$)

When the system damping ratio $\xi = 1$, Eq (8) has two equal real roots:

$$p_1 = p_2 = \frac{1}{T_1} = \frac{1}{T_2} = \omega_n = \frac{1}{T} \tag{17}$$

Similar to overdamping, the dynamic response time of the flywheel energy storage VSG is $t_s = aT = a / \omega_n$. The output power response of the flywheel energy storage VSG is:

$$\Delta P_{Ve}^*(t) = \Delta P_{Vm}^*[1 - e^{-\omega_n t}(1 + \omega_n t)] \tag{18}$$

According to the calculation process under overdamping, the maximum flywheel energy storage required for the VSG rotor motion process under critical damping is $\frac{2\xi}{\omega_n}\Delta P_{Vm}^*$, and the maximum value of the required energy storage power support is $\Delta P_{Vm}^*$.

3) Underdamping ($0 < \xi < 1$)

When the system damping ratio is $0 < \xi < 1$, Eq (8) has two complementary characteristic roots:

$$\begin{cases} p_1 = -(\xi - \sqrt{1 - \xi^2}i)\omega_n \\ p_2 = -(\xi + \sqrt{1 - \xi^2}i)\omega_n \end{cases} \tag{19}$$

The dynamic response of the flywheel energy storage VSG output power is:

$$\Delta P_{Ve}^*(t) = \Delta P_{Vm}^* - \Delta P_{Vm}^* \frac{1}{\sqrt{1-\xi^2}} e^{-\xi\omega_n t} \sin(\omega_d t + \theta) \tag{20}$$

where:

$$\begin{cases} \omega_d = \sqrt{1 - \xi^2}\omega_n \\ \theta = \arctan\left(\frac{\sqrt{1-\xi^2}}{\xi}\right) \end{cases} \tag{21}$$

When underdamped, the output power of the flywheel energy storage VSG will have an overshoot oscillation response, and the response time to reach the steady state for the first time is $\pi - \theta / \omega_d$. At this time, the energy storage and energy storage power support required for the flywheel energy storage VSG rotor movement reach the maximum values of $\frac{2\xi}{\omega_n}\Delta P_{Vm}^*$ and $\Delta P_{Vm}^*$, respectively.

**Table 1.** The parameters of the flywheel energy storage VSG.

| Flywheel energy storage VSG parameters | Value |
|---|---|
| Rated angular frequency (rad/s) | 314 |
| Virtual inertia coefficient $H_{VSG}$/p.u. | 0.15 ($\xi$ = 4); 0.15 ($\xi$ = 1); 0.21 ($\xi$ = 0.707) |
| Damping coefficient $D_{VSG}$/p.u. | 50.24 ($\xi$ = 4); 12.56 ($\xi$ = 1); 12.56 ($\xi$ = 0.707) |
| VSG whole machine synchronous power factor $S_E$/p.u. | 1.03 |

Based on the above analysis, the dynamic response of the flywheel energy storage system VSG shown in Figure 1 is simulated. It is assumed that the capacity of the flywheel energy storage system

is 2.5 MW/0.5 MWh, and it consists of ten 250 kW/50 kWh flywheel energy storage units. Each unit has an independent machine-side converter, and the entire array is connected to the grid through a grid-side converter. The grid-side converter adopts VSG control, and the set system parameters are shown in Table 1.

According to Section 2.2, the flywheel energy storage VSG response model is established. When the power disturbance command is 0.1 p.u., the frequency and output power dynamic responses of the flywheel energy storage VSG under different damping conditions are obtained as shown in Figures 5 and 6. Here, the base value of power is 2.5 MW, and the base value of frequency is 50 Hz.

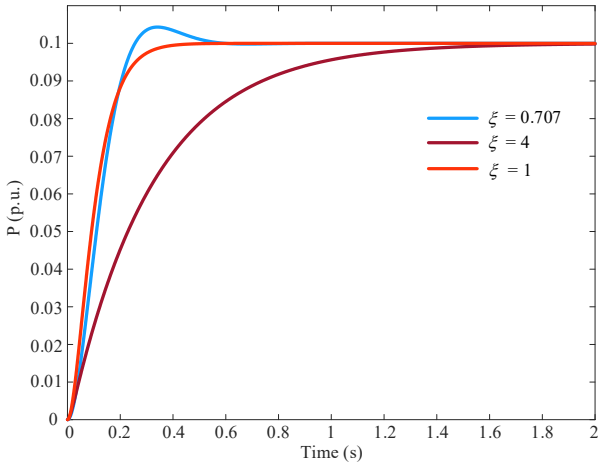


**Figure 5.** Flywheel energy storage VSG dynamic response power model.

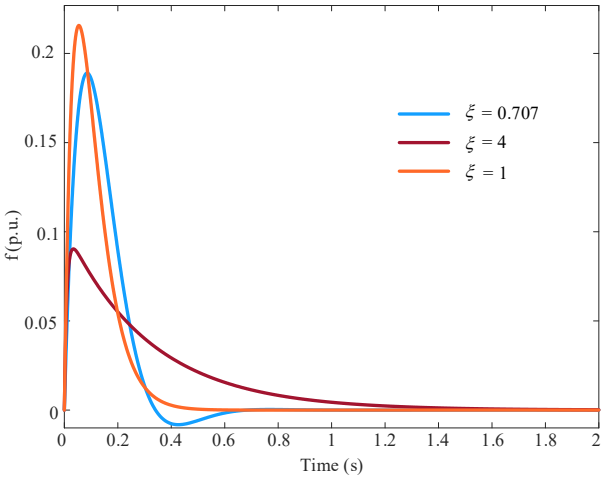


**Figure 6.** Flywheel energy storage VSG dynamic response frequency model.

To support the rotor movement of the flywheel energy storage VSG, the flywheel energy storage can respond in time under different damping ratios. The response speed of the flywheel energy storage VSG is within seconds, and the response speed under critical damping and under-damping conditions is at the millisecond level. The power change of the system is quickly smoothed to a stable state, giving full play to the advantage of the flywheel energy storage system's fast power response speed. When the damping ratio is 0.707, the flywheel energy storage VSG has a faster dynamic response, a smaller overshoot, and the best comprehensive response effect.

## 3. Derivation of the mathematical model of the wind turbine

The modeling of wind turbines includes four parts: The wind turbine model, the transmission shaft model, the generator and the grid-connected converter model. The wind turbine converts wind energy into mechanical energy; the transmission shaft transmits mechanical energy to the generator and the generator and grid-connected converter convert mechanical energy into electrical energy and feed it into the grid.

This paper assumes that (1) The wind turbine operates in MPPT mode; (2) The pitch angle is kept at 0°; (3) The tip speed ratio is constant at the optimal value $\lambda_{opt}$; (4) The wind turbine power is only related to the wind speed and (5) The maximum power does not exceed the rated power [13].

Based on the above assumptions, the wind turbine mechanical power $P_m$ can be expressed as Eq (22):

$$P_m = \frac{\rho}{2} S C_P\left(\lambda_{\text{opt}}, \beta\right) v_w^3 \tag{22}$$

When the wind turbine shaft stiffness is large enough (shaft stiffness $K_s \geqslant 3.0$ p.u.), the concentrated mass model can be used to describe the shaft characteristics, and its expression is:

$$\left(H_g + H_t\right) \frac{d\omega_r}{dt} = T_m - T_e - D_r \omega_r \tag{23}$$

Assume that the wind turbine uses a permanent magnet synchronous generator (PMSG); its AC power is converted into DC power by the machine-side converter, and then converted into AC power with the same frequency as the grid by the grid-side converter, being connected to the grid.

Taking PMSG as the control object and adopting the control strategy of d-axis current $i_d = 0$, its voltage equation, electromagnetic torque equation, and motion equation in the two-phase rotating coordinate system are as follows:

$$\begin{cases} u_d = -\omega_e L i_q \\ u_q = L \frac{di_q}{\mathrm{dt}} + R_s i_q + \omega_e \psi_f \end{cases} \tag{24}$$

$$T_e = -\frac{3}{2} p \psi_f i_q \tag{25}$$

$$J \frac{d\omega_m}{\mathrm{dt}} = T_e - T_l - B\omega_m \tag{26}$$

The control target of the machine-side converter is to adjust the output active power [14]. Therefore, a dual closed-loop control method of the power outer loop and the current inner loop is adopted. The control principle is shown in Figure 7, where PI refers to the PI controller (proportional-integral controller), SVPWM stands for space vector pulse width modulation, and PMSG denotes the permanent magnet synchronous generator.

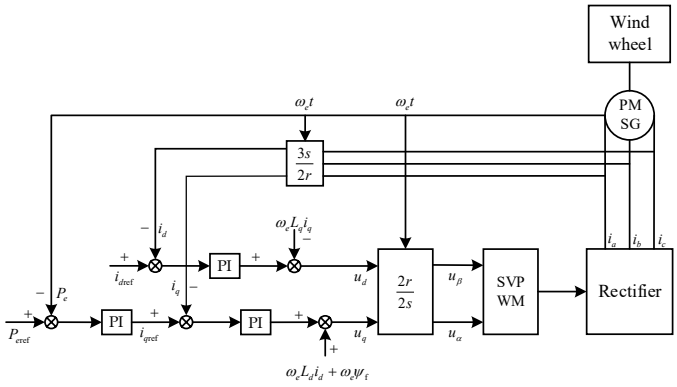


**Figure 7.** Generator-side converter control schematic.

The grid-side converter needs to maintain the DC bus voltage stable to ensure that all active power is fed into the grid. Its control principle is shown in Figure 8.

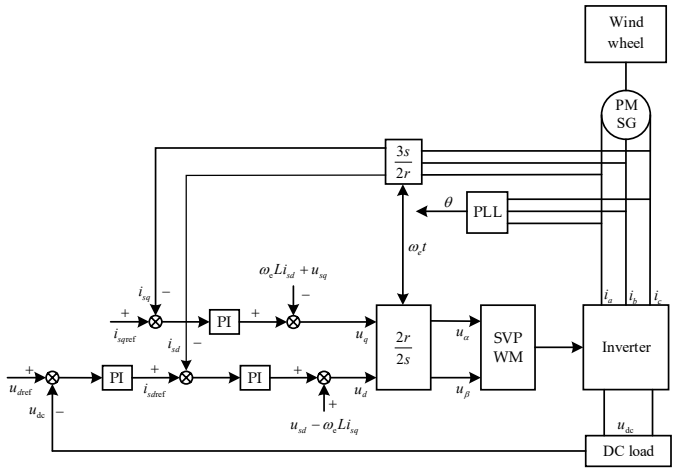


**Figure 8.** Grid-side converter control schematic.

## 4. Simulation analysis

### *4.1. Simulation experiment background*

A certain city is located in a plain and faces the sea to the east. Its coastal tidal flats are rich in wind energy resources and are very suitable for the construction of wind farms. According to statistics, as of September 2022, the installed capacity of renewable energy in the region accounts for about 20%, and the installed capacity of thermal power plants accounts for about 80%. The current installed capacity of renewable energy is growing rapidly, and it is expected to reach 30% in 2025. With the large-scale access to renewable energy, the frequency security issue of the power system has become increasingly prominent. The use of flywheel energy storage VSG technology to assist the operation of offshore wind farms can effectively improve the frequency regulation capability of wind farms, thereby promoting the consumption of renewable energy.

*4.2. Regional frequency control model*

Based on the mathematical model and frequency calculation theory mentioned above, the flywheel energy storage VSG-assisted wind turbine primary frequency regulation regional power grid model can be established as shown in Figure 9.

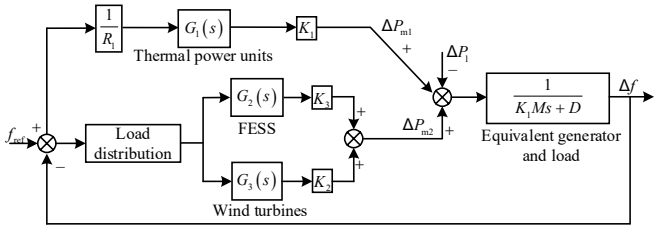


**Figure 9.** Regional power grid primary frequency regulation model.

The comprehensive transfer function of the thermal power unit is shown in Eq (27):

$$G_1(s) = \frac{1+aT_G s}{1+T_G s} \tag{27}$$

The load distribution rule of the joint operation model is as follows: The flywheel energy storage VSG only receives the frequency modulation signal to smooth the frequency fluctuation and does not bear the conventional load; the wind turbine does not receive the frequency modulation signal and only adjusts the power generation according to the external wind speed change.

*4.3. Simulation experiment*

**Table 2.** Flywheel energy storage system simulation parameter table.

| Parameter | Value |
|---|---|
| $R_1$ | 0.05 |
| $T_G$ (s) | 6 |
| $a$ | 0.33 |
| $M$ (s) | 10 |
| $D$ | 1 |
| $H_{SVG}$ | 0.05 |
| $D_{SVG}$ | 4 |
| $K_1$ | 0.64 |
| $K_2$ | 0.32 |
| $K_3$ | 0.04 |

The total installed capacity of the regional power grid is 1000 MW, including 800 MW of thermal power and 200 MW of wind power. Assuming that the total installed capacity of wind power increases to 400 MW due to the large-scale construction of wind turbines in coastal tidal flats, a 50 MW flywheel energy storage device is installed to improve the frequency regulation capability of the newly built wind farm. The values of the system parameters are shown in Table 2. In the following text, both power

and frequency are expressed in per unit (p.u.). The base values are specified as follows: The base value of power is 1000 MW, and the base value of frequency is 50 Hz.

This model uses the wind speed data of the actual running wind turbine as input. The measured wind speed curve of a wind turbine is shown in Figure 10.

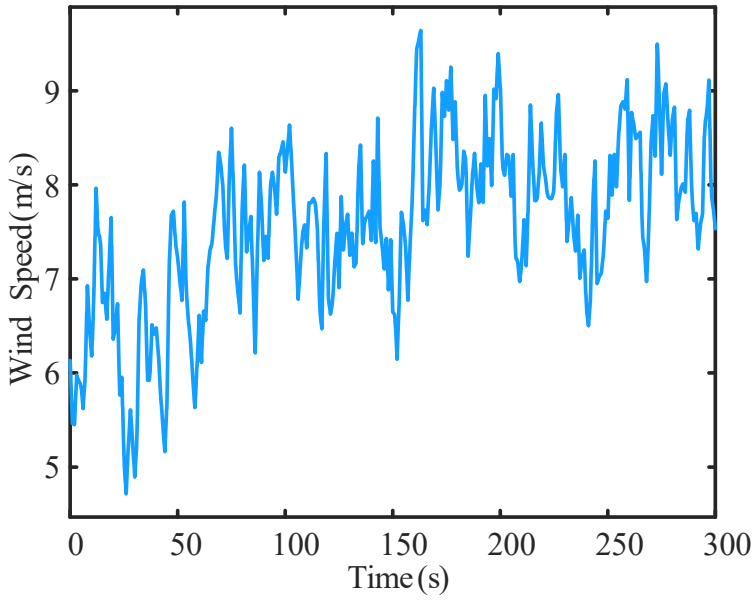


**Figure 10.** Wind speed signal of the fan.

At 150 seconds, a power step disturbance with an amplitude of 0.05 p.u. is applied to the area, and the system frequency responses under different working conditions are shown in Figures 11 and 12. The output power of the flywheel energy storage system and the thermal power generating units are shown in Figure 13. The experimental result data are presented in Table 3.

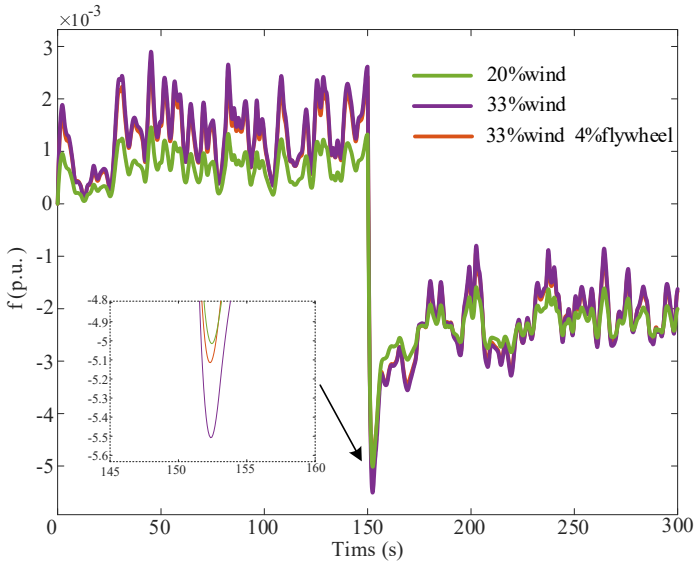


**Figure 11.** Frequency deviation comparison of wind power access areas.

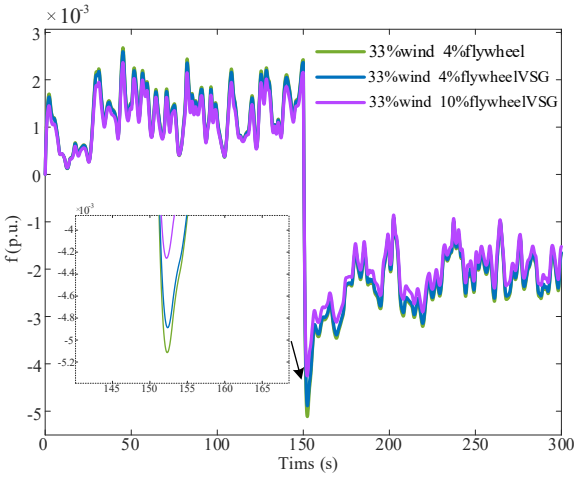


**Figure 12.** Comparison of frequency deviations in frequency regulation regions of flywheel-assisted wind turbines.

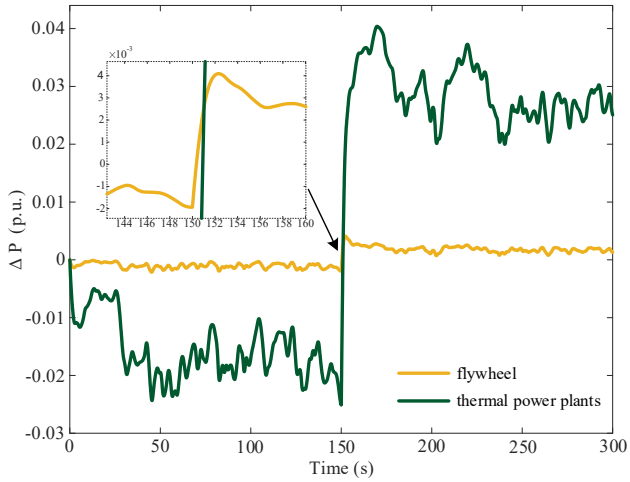


**Figure 13.** Frequency deviation comparison of wind power access areas.

**Table 3.** Flywheel energy storage system simulation parameter table.

| Operating mode | Extremes of frequency deviation | Percentage reduction | Standard deviation of frequency deviation | Percentage reduction |
|---|---|---|---|---|
| 20% wind | $-5.02 \times 10^{-3}$ p.u. | — | $1.59 \times 10^{-3}$ p.u. | — |
| 33% wind | $-5.51 \times 10^{-3}$ p.u. | — | $1.97 \times 10^{-3}$ p.u. | — |
| 33% wind 4% flywheel | $-5.11 \times 10^{-3}$ p.u. | 7.26 | $1.91 \times 10^{-3}$ p.u. | 3.05 |
| 33% wind 4% flywheelVSG | $-4.89 \times 10^{-3}$ p.u. | 11.25 | $1.87 \times 10^{-3}$ p.u. | 5.08 |
| 33% wind 10% flywheelVSG | $-4.26 \times 10^{-3}$ p.u. | 22.69 | $1.72 \times 10^{-3}$ p.u. | 12.69 |

According to Figures 11–12 and Table 3, the following conclusions can be drawn:

1) In regional power grids with a high wind power share, the randomness and volatility of wind power output will have a huge impact on the grid frequency, and its impact even exceeds the user-side load disturbance.

2) As the proportion of wind turbine generation increases, the frequency characteristics of the regional power grid deteriorate. After the proportion of wind power increases by 12%, the extreme value of the regional power grid frequency deviation increases by about 10% (extreme values of frequency under the 33% wind power operating condition compared with those under the 20% wind power operating condition), and the standard deviation increases by 24% (standard deviation of frequency under the 33% wind power operating condition compared with that under the 20% wind power operating condition), which can easily cause the grid frequency to exceed the safe operating range.

3) The addition of flywheel energy storage can effectively alleviate the frequency safety problem caused by the increase in wind power share. Configuring 4% capacity of flywheel energy storage can reduce the extreme value of regional power grid frequency deviation by about 8% and the standard deviation by 3%.

4) The operation mode of the flywheel energy storage system enhanced by VSG technology exhibits superior frequency regulation performance. Under the condition of the same capacity, the FESS adopting the VSG control mode can reduce the extreme value of the regional power grid frequency deviation by approximately 4% (from $-5.11 \times 10^{-3}$ p.u. to $-4.89 \times 10^{-3}$ p.u.) and decrease the standard deviation of frequency deviation by 2% (from $1.91 \times 10^{-3}$ p.u. to $1.87 \times 10^{-3}$ p.u.). Furthermore, by optimizing the virtual operation parameters of the VSG, the frequency regulation effect will be further improved.

5) As the capacity of the flywheel energy storage system increases, its frequency control effect on the regional power grid continues to improve. Compared with the 4% capacity solution, the 10% capacity flywheel energy storage can further reduce the frequency deviation extreme value by about 15% and the standard deviation by 8.77%.

To verify the above conclusions, a randomly generated continuous disturbance signal is applied to the regional power grid (as shown in Figure 14).

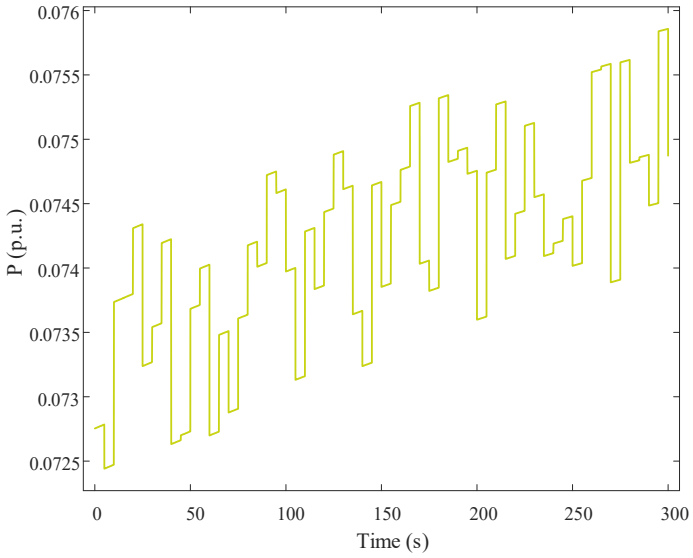


**Figure 14.** Continuous disturbance signal.

Under given load disturbance conditions, the system frequency response characteristics are shown in Figures 15 and 16. The experimental result data are presented in Table 4.

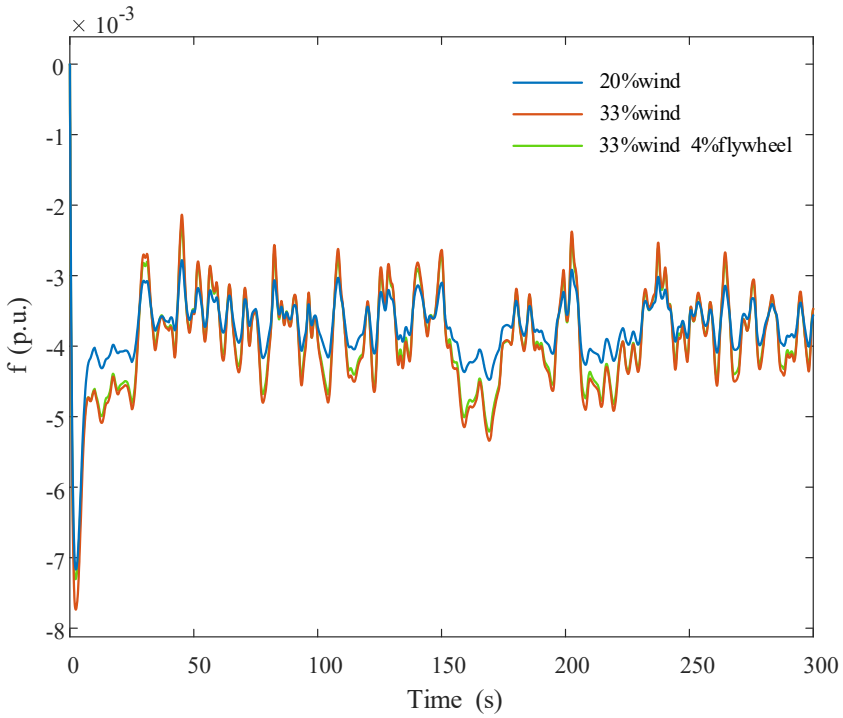


**Figure 15.** Frequency deviation comparison of continuous disturbance wind power access conditions.

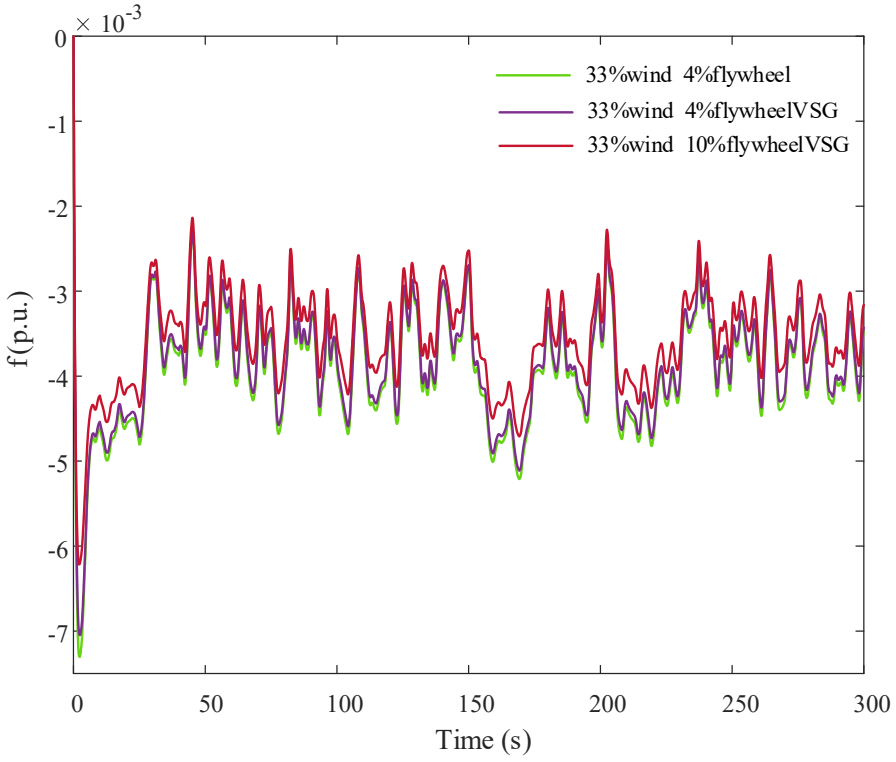


**Figure 16.** Comparison of regional frequency deviations under continuous disturbance flywheel-assisted wind turbine frequency regulation conditions.

**Table 4.** Flywheel energy storage system simulation parameter table.

| Operating mode | Extremes of frequency deviation | Percentage reduction | Standard deviation of frequency deviation | Percentage reduction |
|---|---|---|---|---|
| 20% wind | $-7.17 \times 10^{-3}$ p.u. | — | $4.89 \times 10^{-4}$ p.u. | — |
| 33% wind | $-7.74 \times 10^{-3}$ p.u. | — | $7.42 \times 10^{-4}$ p.u. | — |
| 33% wind 4% flywheel | $-7.30 \times 10^{-3}$ p.u. | 5.68 | $6.79 \times 10^{-4}$ p.u. | 8.49 |
| 33% wind 4% flywheelVSG | $-7.05 \times 10^{-3}$ p.u. | 8.91 | $6.57 \times 10^{-3}$ p.u. | 11.46 |
| 33% wind 10% flywheelVSG | $-6.22 \times 10^{-3}$ p.u. | 19.64 | $5.81 \times 10^{-3}$ p.u. | 21.70 |

Under the action of a continuous disturbance signal, the following conclusions are consistent with the previous results:

1) When the proportion of wind power increases by 12%, the standard deviation of the regional power grid frequency deviation increases by 51%.

2) After configuring flywheel energy storage with a capacity of 4%, the standard deviation of the frequency deviation decreases by 4%.

3) The standard deviation of the frequency deviation can be further reduced by 3% by adopting the VSG operation mode.

4) Under 10% flywheel energy storage capacity with VSG working condition, the standard deviation of the frequency deviation is cumulatively reduced by 11%.

These conclusions are consistent with the results of the step disturbance analysis mentioned above.

## 5. Conclusions

This paper studies the impact of flywheel energy storage and VSG-assisted wind turbine frequency regulation on grid frequency under the increasing penetration of large-scale renewable energy. By establishing a Matlab/Simulink simulation model of flywheel energy storage with VSG-assisted frequency regulation, the following conclusions are drawn:

1) In regional power grids, the increase in the proportion of wind turbine power generation will have a significant impact on system frequency security, and the use of the flywheel energy storage system to assist wind turbine frequency regulation can effectively mitigate this impact.

2) The flywheel energy storage system has more advantages in VSG operation mode than conventional operation mode, due to adjustable parameters and enhanced flexibility.

3) The flywheel energy storage system with a larger capacity has stronger frequency regulation performance. However, considering the high unit cost of flywheel energy storage, its configuration capacity needs to be rigorously calculated.

## Use of AI tools declaration

The authors declare they have not used Artificial Intelligence (AI) tools in the creation of this article.

## Acknowledgments

The authors highly thank Shenzhen Energy Group for providing essential research support.

## Conflict of interest

The authors declare no conflicts of interest.

## Author contributions

All authors contributed equally to this work. Conceptualization, Wang L.; methodology, Wang L; software, Qiao T; validation, Chen C; formal analysis, Chen C; investigation, Wang L; resources, Wang L; data curation, Zhao Y; writing—original draft preparation, Wang L; writing—review and editing, Liu Y; visualization, Chen C.

## References


1. Rapizza MR, Canevese SM, Cirio D (2022) Grid frequency control: Interaction between fast regulations. *2022 AEIT International Annual Conference (AEIT)*, 1–6. https://doi.org/10.23919/AEIT56783.2022.9951801
2. Cheng Y, Azizipanah-Abarghooee R, Azizi S, et al. (2020) Smart frequency control in low inertia energy systems based on frequency response techniques: A review. *Appl Energy* 279: 115798. https://doi.org/10.1016/j.apenergy.2020.115798
3. Mallemaci V, Mandrile F, Rubino S, et al. (2021) A comprehensive comparison of virtual synchronous generators with focus on virtual inertia and frequency regulation. *Electr Power Syst Res* 201: 107516. https://doi.org/10.1016/j.epsr.2021.107516
4. Othman MH, Mokhlis H, Mubin M, et al. (2020) Progress in control and coordination of energy storage system-based VSG: A review. *IET Renewable Power Gener* 14: 177–187. https://doi.org/10.1049/iet-rpg.2019.0274
5. Liang J, Fan H, Cheng L, et al. (2024) Control strategy for improving the frequency response characteristics of photovoltaic and energy storage systems based on VSG control. *Energy Rep* 11: 2295–2305. https://doi.org/10.1016/j.egyr.2024.01.036
6. Chen S, Sun Y, Han H, et al. (2023) A modified VSG control scheme with virtual resistance to enhance both small-signal stability and transient synchronization stability. *IEEE Trans Power Electron* 38: 6005–6014. https://doi.org/10.1109/TPEL.2023.3243025
7. Chen S, Sun Y, Hou X, et al. (2023) Quantitative parameters design of VSG oriented to transient synchronization stability. *IEEE Trans Power Electron* 38: 4978–4981. https://doi.org/10.1109/TPWRS.2023.3293016
8. Li H, Wang X, Li Y, et al. (2025) Design of flywheel energy storage device with high specific energy. *AIMS Energy* 13: 781–797. https://doi.org/10.3934/energy.2025028
9. Ji W, Hong F, Zhao Y, et al. (2024) Applications of flywheel energy storage system on load frequency regulation combined with various power generations: A review. *Renewable Energy* 223: 119975. https://doi.org/10.1016/j.renene.2024.119975
10. Tziovani L, Hadjidemetriou L, Charalampous C, et al. (2021) Energy management and control of a flywheel storage system for peak shaving applications. *IEEE Trans Smart Grid* 12: 4195–4207. https://doi.org/10.1109/TSG.2021.3084814

11. Zhu Y, Wang H, Zhu Z (2021) Improved VSG control strategy based on the combined power generation system with hydrogen fuel cells and supercapacitors. *Energy Rep* 7: 6820–6832. https://doi.org/10.1016/j.egyr.2021.10.056
12. Li M, Shu S, Wang Y, et al. (2022) Analysis and improvement of large-disturbance stability for grid-connected VSG based on output impedance optimization. *IEEE Trans Power Electron* 37: 9807–9826. https://doi.org/10.1109/TPEL.2022.3153563
13. Kumar D, Chatterjee K (2016) A review of conventional and advanced MPPT algorithms for wind energy systems. *Renewable Sustainable Energy Rev* 55: 957–970. https://doi.org/10.1016/j.rser.2015.11.013
14. Liu Z, Cheng X, Peng X, et al. (2024) A review of common-mode voltage suppression methods in wind power generation. *Renewable Sustainable Energy Rev* 203: 114773. https://doi.org/10.1016/j.rser.2024.114773


AIMS Press